William Morrish, Peter West, Nathan Orlando, Elizaveta Klantsataya, Kirsty Gardner, Stephen Lane, Raymond Decorby, Alexandre François, and Alkiviathes Meldrum
Refractometric micro-sensor using a mirrored capillary resonator
Optics Express, 2016; 24(22):24959-24970

Published version http://dx.doi.org/10.1364/OE.24.024959

Research Article | Vol. 24, No. 22 | 31 Oct 2016 | OPTICS EXPRESS 24959

Optics EXPRESS

Refractometric micro-sensor using a mirrored capillary resonator

WILLIAM MORRISH,[1] PETER WEST,[1] NATHAN ORLANDO,[1] ELIZAVETA KLANTSATAYA,[2] KIRSTY GARDNER,[1] STEPHEN LANE,[1] RAYMOND DECORBY,[3] ALEXANDRE FRANÇOIS,[2,4] AND ALKIVIATHES MELDRUM[1,*]

[1]*Department of Physics, University of Alberta, Edmonton, AB T6G2E1, Canada*
[2]*The Institute for Photonics and Advanced Sensing (IPAS), School of Physical Sciences, The University of Adelaide, SA 5005 Adelaide, Australia*
[3]*Department of Electrical and Computer Engineering, University of Alberta, Edmonton, AB T6G2V4, Canada*
[4]*School of Engineering, University of South Australia, SA 5000 Adelaide, Australia*
[*]*ameldrum@ualberta.ca*

Abstract: We report on a flow-through optical sensor consisting of a microcapillary with mirrored channels. Illuminating the structure from the side results in a complicated spectral interference pattern due to the different cavities formed between the inner and outer capillary walls. Using a Fourier transform technique to isolate the desired channel modes and measure their resonance shift, we obtain a refractometric detection limit of $(6.3 \pm 1.1) \times 10^{-6}$ RIU near a center wavelength of 600 nm. This simple device demonstrates experimental refractometric sensitivities up to $(5.6 \pm 0.2) \times 10^{2}$ nm/RIU in the visible spectrum, and it is calculated to reach 1540 nm/RIU with a detection limit of 2.3×10^{-6} RIU at a wavelength of 1.55 μm. These values are comparable to or exceed some of the best Fabry-Perot sensors reported to date. Furthermore, the device can function as a gas or liquid sensor or even as a pressure sensor owing to its high refractometric sensitivity and simple operation.

OCIS codes: (070.5753) Resonators; (050.2230) Fabry-Perot; (280.4788) Optical sensing and sensors; (300.6300) Spectroscopy, Fourier transforms.

References and links

1. X. Fan and I. M. White, "Optofluidic microsystems for chemical and biological analysis," Nat. Photonics **5**(10), 591–597 (2011).
2. J. Jágerská, H. Zhang, Z. Diao, N. L. Thomas, and R. Houdré, "Refractive index sensing with an air-slot photonic crystal nanocavity," Opt. Lett. **35**(15), 2523–2525 (2010).
3. H. Clevenson, P. Desjardins, X. T. Gan, and D. Englund, "High sensitivity gas sensor based on high-Q suspended polymer photonic crystal nanocavity," Appl. Phys. Lett. **104**(24), 241108 (2014).
4. M. R. Foreman, J. D. Swaim, and F. Vollmer, "Whispering gallery mode sensors," Adv. Opt. Photonics **7**(2), 168–240 (2015).
5. Y.-J. Rao, M. Deng, D.-W. Duan, X.-C. Yang, T. Zhu, and G.-H. Cheng, "Micro Fabry-Perot interferometers in silica fibers machined by femtosecond laser," Opt. Express **15**(21), 14123–14128 (2007).
6. A. François, Y. Zhi, and A. Meldrum, "Whispering Gallery Mode Devices for Sensing and Biosensing," in *Photonic Materials for Sensing, Biosensing, and Display Devices* (Springer Series in Materials Science, 2016) pp. 237–288.
7. T. Reynolds, M. R. Henderson, A. François, N. Riesen, J. M. Hall, S. V. Afshar, S. J. Nicholls, and T. M. Monro, "Optimization of whispering gallery resonator design for biosensing applications," Opt. Express **23**(13), 17067–17076 (2015).
8. Y. G. Zhang, S. B. Han, S. L. Zhang, P. H. Liu, and Y. C. Shi, "High-Q and High-Sensitivity Photonic Crystal Cavity Sensor," IEEE Photonics J. **7**(5), 6802906 (2015).
9. R. St-Gelais, J. Masson, and Y. A. Peter, "All-silicon integrated Fabry-Perot cavity for volume refractive index measurement in microfluidic systems," Appl. Phys. Lett. **94**(24), 243905 (2009).
10. T. Wei, Y. Han, Y. Li, H. L. Tsai, and H. Xiao, "Temperature-insensitive miniaturized fiber inline Fabry-Perot interferometer for highly sensitive refractive index measurement," Opt. Express **16**(8), 5764–5769 (2008).
11. C. P. K. Manchee, V. Zamora, J. W. Silverstone, J. G. C. Veinot, and A. Meldrum, "Refractometric sensing with fluorescent-core microcapillaries," Opt. Express **19**(22), 21540–21551 (2011).

#272716 http://dx.doi.org/10.1364/OE.24.024959
Journal © 2016 Received 29 Jul 2016; revised 6 Oct 2016; accepted 11 Oct 2016; published 17 Oct 2016

Optics EXPRESS

12. Y. Zhi, T. Thiessen, and A. Meldrum, "Silicon quantum dot coated microspheres for microfluidic refractive index sensing," J. Opt. Soc. Am. B **30**(1), 51–56 (2013).
13. S. Pang, R. E. Beckham, and K. E. Meissner, "Quantum dot-embedded microspheres for remote refractive index sensing," Appl. Phys. Lett. **92**(22), 221108 (2008).
14. P. Zijlstra, K. L. van der Molen, and A. P. Mosk, "Spatial refractive index sensor using whispering gallery modes in an optically trapped microsphere," Appl. Phys. Lett. **90**(16), 161101 (2007).
15. A. François, N. Riesen, H. Ji, S. Afshar V, and T. M. Monro, "Polymer based whispering gallery mode laser for biosensing applications," Appl. Phys. Lett. **106**(3), 031104 (2015).
16. I. M. White and X. Fan, "On the performance quantification of resonant refractive index sensors," Opt. Express **16**(2), 1020–1028 (2008).
17. H. Y. Choi, K. S. Park, S. J. Park, U.-C. Paek, B. H. Lee, and E. S. Choi, "Miniature fiber-optic high temperature sensor based on a hybrid structured Fabry-Perot interferometer," Opt. Lett. **33**(21), 2455–2457 (2008).
18. D.-W. Duan, Y. J. Rao, Y.-S. Hou, and T. Zhu, "Microbubble based fiber-optic Fabry-Perot interferometer formed by fusion splicing single-mode fibers for strain measurement," Appl. Opt. **51**(8), 1033–1036 (2012).
19. C. R. Liao, T. Y. Hu, and D. N. Wang, "Optical fiber Fabry-Perot interferometer cavity fabricated by femtosecond laser micromachining and fusion splicing for refractive index sensing," Opt. Express **20**(20), 22813–22818 (2012).
20. Y. Guo, H. Li, K. Reddy, H. S. Shelar, V. R. Nittoor, and X. Fan, "Optofluidic Fabry–Pérot cavity biosensor with integrated flow-through micro-/nanochannels," Appl. Phys. Lett. **98**(4), 041104 (2011).
21. W. Z. Song, X. M. Zhang, A. Q. Liu, C. S. Lim, P. H. Yap, and H. M. M. Hosseini, "Refractive index measurement of single living cells using on-chip Fabry-Pérot cavity," Appl. Phys. Lett. **89**(20), 203901 (2006).
22. S. Calixto, M. Rosete-Aguilar, D. Monzon-Hernandez, and V. P. Minkovich, "Capillary refractometer integrated in a microfluidic configuration," Appl. Opt. **47**(6), 843–848 (2008).
23. H. El Ghandoor, E. Hegazi, I. Nasser, and G. M. Behery, "Measuring the refractive index of crude oil using a capillary tube interferometer," Opt. Laser Technol. **35**(5), 361–367 (2003).
24. B. Krattiger, A. E. Bruno, H. M. Widmer, M. Geiser, and R. Dändliker, "Laser-Based Refractive-Index Detection for Capillary Electrophoresis: Ray-Tracing Interference Theory," Appl. Opt. **32**(6), 956–965 (1993).
25. S. Qi, X. Yang, C. Zhang, L. Zhang, X. Wang, T. Xu, J. Tian, and G. Zhang, "Analysis of capillary interferometry for measuring refractive indices of minute samples," Appl. Opt. **43**(3), 530–536 (2004).
26. H. J. Tarigan, P. Neill, C. K. Kenmore, and D. J. Bornhop, "Capillary-Scale Refractive Index Detection by Interferometric Backscatter," Anal. Chem. **68**(10), 1762–1770 (1996).
27. A. Yang, W. Li, G. Yuan, J. Dong, and J. Zhang, "Measuring the refractive indices of liquids with a capillary tube interferometer," Appl. Opt. **45**(31), 7993–7998 (2006).
28. S. Surdo, S. Merlo, F. Carpignano, L. M. Strambini, C. Trono, A. Giannetti, F. Baldini, and G. Barillaro, "Optofluidic microsystems with integrated vertical one-dimensional photonic crystals for chemical analysis," Lab Chip **12**(21), 4403–4415 (2012).
29. S. Surdo, F. Carpignano, L. M. Strambini, S. Merlo, and G. Barillaro, "Capillarity-driven (self-powered) one-dimensional photonic crystals for refractometry and (bio)sensing applications," RSC Advances **4**(94), 51935–51941 (2014).
30. O. Svelto, S. Longhi, G. Della Valle, S. Kuck, G. Hiuber, M. Pollnau, H. Hillmer, S. Hansmann, R. Engelbrecht, H. Brand, J. Kaiser, A. B. Peterson, R. Malz, S. S. G. Marawsky, U. Brinkmann, D. Lot, A. Borsutzky, H. Wachter, M. W. Sigrist, S. E. E. Schneidmiller, M. Yurkov, K. Midorikawa, J. Hein, R. Sauerbrey, and J. Helmcke, eds., *Lasers and Coherent Light Sources*, Springer Handbook of Lasers and Optics (Springer, 2007), p. 354.
31. http://www.polysciences.com/default/pentabromophenyl-acrylate.
32. X. Wei and D. K. Roper, "Tin Sensitization for Electroless Plating Review," J. Electrochem. Soc. **161**(5), D235–D242 (2014).
33. E. Klantsataya, A. François, H. Ebendorff-Heidepriem, B. Sciacca, A. Zuber, and T. M. Monro, "Effect of surface roughness on metal enhanced fluorescence in planar substrates and optical fibers," Opt. Mater. Express **6**(6), 2128 (2016).
34. J. W. Silverstone, S. McFarlane, C. P. K. Manchee, and A. Meldrum, "Ultimate resolution for refractometric sensing with whispering gallery mode microcavities," Opt. Express **20**(8), 8284–8295 (2012).
35. Y. Clergent, C. Durou, and M. Laurens, "Refractive index variations for argon, nitrogen, and carbon dioxide at lambda = 632.8 nm (He-Ne laser light) in the range 288.15K <= T <= 323.15K, 0 < p < 110 kPa," J. Chem. Eng. Data **44**(2), 197–199 (1999).
36. F. Carpignano, G. Rigamonti, T. Migliazza, and S. Merlo, "Refractive Index Sensing in Rectangular Glass Micro-Capillaries by Spectral Reflectivity Measurements," IEEE J. Sel. Top. Quantum Electron. **22**(3), 7100309 (2016).
37. M. Piliarik and J. Homola, "Surface plasmon resonance (SPR) sensors: approaching their limits?" Opt. Express **17**(19), 16505–16517 (2009).
38. G. Liu and M. Han, "Fiber-optic gas pressure sensing with a laser-heated silicon-based Fabry-Perot interferometer," Opt. Lett. **40**(11), 2461–2464 (2015).
39. B. Xu, C. Wang, D. N. Wang, Y. Liu, and Y. Li, "Fiber-tip gas pressure sensor based on dual capillaries," Opt. Express **23**(18), 23484–23492 (2015).

Optics EXPRESS

40. É. Pinet, "Pressure measurement with fiber-optic sensors: commercial technologies and applications," Proc. SPIE **7753**, 775304 (2011).
41. Y. Z. Zhu, K. L. Cooper, G. R. Pickrell, and A. Wang, "High-temperature fiber-tip pressure sensor," J. Lightwave Technol. **24**(2), 861–869 (2006).
42. http://www.crystran.co.uk/optical-materials/silica-glass-sio2.
43. W. B. Emerson, "Compressibility of fused-quartz glass at atmopsheric pressure," J. Res. Natl. Bur. Stand. **18**(6), 683–711 (1937).
44. S. B. Sane and W. G. Knauss, "The Time-Dependent Bulk Response of Poly (Methyl Methacrylate)," Mech. Time-Depend. Mater. **5**(4), 293–324 (2001).
45. J. Xie, S. de Gironcoli, S. Baroni, and M. Scheffler, "First-principles calculation of the thermal properties of silver," Phys. Rev. B **59**(2), 965–969 (1999).
46. J. Mai, V. V. Abhyankar, M. E. Piccini, J. P. Olano, R. Willson, and A. V. Hatch, "Rapid detection of trace bacteria in biofluids using porous monoliths in microchannels," Biosens. Bioelectron. **54**, 435–441 (2014).

1. Introduction

Microscale optical sensors could address important needs in fields ranging from health sciences to clean energy development [1]. Optofluidic architectures are especially interesting in this context, providing a strong interaction between the probing light and the analyte [1]. Many optofluidic sensors utilize interference effects in which the path length of light within the device is affected by the properties of the analyte medium. Notable types of microscale interference-based sensors include photonic crystal cavities (PCCs) (e.g., Ref [2].) that can act as gas sensors [3], whispering gallery mode (WGM) structures [4], and microscale Fabry-Pérot (FP) interferometers [5].

In all these devices, the presence of the analyte causes a change in the local refractive index (RI), which in turn causes a shift in the resonance frequencies. The sensitivity to RI changes in the analyte is typically measured in wavelength shift (nm) per refractive index "unit" (nm/RIU). In WGM-based devices, the sensitivity depends on a variety of experimental parameters and is typically in the range of 5-50 nm/RIU [6,7]. In PCCs, one can obtain sensitivities as high as 500 nm/RIU [8]. FP interferometers typically have the highest sensitivities because the electric field is predominantly in the analyte region, with values up to 900 nm/RIU [9] or even 1160 nm/RIU [10] as recently reported at a wavelength of 1550 nm.

The limit of detection (LoD) represents the minimum detectable refractive index change. Current typical LoDs are somewhat difficult to summarize coherently since they are almost always extrapolated from much larger RI changes. For fluorescence WGM-based refractive-index sensors, estimated LoDs are typically in the range of 10^{-3} – 10^{-4} RIU [11–15]. These values can be pushed down to 10^{-5} RIU for PCC gas sensors [2] or ~10^{-6} RIU for evanescently-coupled microspheres and other WGM-type structures [16]. However, these devices can be difficult and/or expensive to prepare and often require expensive precision equipment to be operated, making them impractical for many applications. For example, micron-scale Fabry-Pérot cavities on optical fibers are often fabricated using femtosecond machining [5,10], fusion splicing different fibers [17,18], or a mix of both [19]. Alternatively, two fiber or waveguide tips with a reflective coating can be positioned in close proximity to form the FP cavity in a flow-through microchannel [20,21].

Here, we demonstrate a simple capillary-based microfluidic sensor, which doesn't require any micromachining or any other complex microfabrication techniques, with a sensitivity as high as $(5.6 \pm 0.2) \times 10^2$ nm/RIU in the visible spectrum, corresponding to ~1540 nm/RIU at a wavelength of 1550 nm, and demonstrate its usage for chemical or pressure sensing. The light scattering and interference pattern from capillaries has been investigated for refractometric applications before [22–27]; here we instead employ the cylindrical FP resonances for sensitive refractometric shift sensing, which is somewhat more reminiscent of the optofluidic photonic crystal cavities reported in [28,29]. Two different approaches have been pursued to increase the reflectivity of the inner capillary walls, resulting in higher cavity quality (Q) factor. The first approach uses a high refractive index polymer coating, enabling resonances with a sufficiently high visibility and Q to be observed in an all-dielectric

Optics EXPRESS

structure due to the high refractive index contrast between the channel medium and the deposited polymer layer. The second method used involves the deposition of a silver thin film, using an electroless plating method, onto the inner capillary wall to produce a partially transparent silver mirror. While the latter structure is clearly lossier, the reflectivity of the channel mirrors can be significantly higher than in the polymer case, resulting in clearly distinguishable resonances.

2. Basic structure

The devices consisted of channel-coated microcapillaries into which broadband radiation from a tungsten lamp was directed perpendicular to the capillary axis [Fig. 1]. It was impractical to measure an insertion loss, but as the incident beam was roughly parallel and not narrowly focused onto the capillary, the percentage of incident radiation coupled into the channel was certainly low; despite this the signal intensity was more than sufficient. In this orientation, the capillary can be viewed as two concentric, low-finesse cylindrical FP cavities with the distance between the mirrors (L) being twice the radius R. There are four interfaces perpendicular to the capillary axis (labeled 1 to 4 on Fig. 1) which form sets of different FP cavities. The strongest resonances will correspond to those having the highest reflection coefficients and longest cavity lengths. Of particular importance is the cavity formed between interfaces 2-3 [Fig. 1]; because most of the field is contained within the channel it should have the highest sensitivity to the channel media. Cavity (2-3) also forms a marginally stable resonator similar to cavity (1-4) (both have a radius of curvature R equal to half the channel length L). Additional resonances would also exist within the thin mirror layer, but this long-wavelength periodicity is not observable within the ~60-nm wavelength range of our spectrometer.

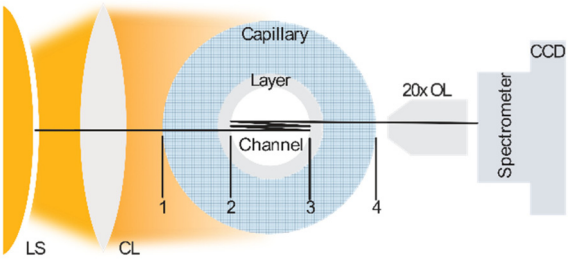

Fig. 1. Diagram illustrating the basic structure of the capillary and the experimental setup. Light from the tungsten lamp (LS) was roughly collimated using a condenser lens (CL). A 20x objective lens (OL) was used to collect the transmitted radiation and pass it to an imaging CCD spectrometer with a nominal resolving power of 2800. Continuous exposures of 30 seconds each were taken for sensorgram measurements. Capillary interfaces 1, 2, 3, and 4 are labeled. The channel layer thickness is greatly exaggerated for clarity.

In a cylindrical cavity of length $L = 2R$, where R is the radius, the transverse modes are degenerate and the mode spacing is simply given by $\Delta f = c/(2n_{eff}L)$, where c is the speed of light in vacuum, L is the cavity length (the diameter in this case), and n_{eff} is the effective index, which is analogous to an FP cavity of the same length [30]. The quality factor is approximately $Q = (2\pi L/(-\lambda \cdot Ln[R]))$ ignoring diffraction losses, where R is the reflectance. For the high-index polymer-coated capillary, the calculated Q-factor is ~200 for the modes defined by interfaces 2-3 (which we will refer to as "channel modes") with air in the channel. In contrast, the air-glass outer interface (cavity 1-4) has a predicted Q of ~1400. This difference is mainly due to the much larger length of the (1-4) cavity.

With a silver-mirrored channel, the reflection coefficients and Q-factors depend on the mirror thickness. For example, for a 30-nm coating the reflection coefficient is 0.88 and the calculated Q-factor is ~4000. Obviously the Q-factor would improve with coating thickness, but thick mirrors reduce the transmission through the device.

Optics EXPRESS

3. Device fabrication and characterization

The microfluidic FP cavities were prepared using fused silica microcapillaries (RI = 1.45) from Polymicro Technologies or Beckman-Coulter, with inner and outer diameters of 50 and 320 μm, respectively. The 20-μm jackets were removed by ashing at 650 °C.

Poly(penta-bromophenyl)acrylate (ppba; Sigma) was chosen as the polymer to be deposited onto the capillary inner wall due to its high refractive index (n~1.7) in the visible [31]. The polymer was dissolved into chloroform (1 mg/mL), the resulting solution was allowed to fill the channel by capillary action, and the solvent was then evaporated at ~70 °C for 20 minutes in atmosphere. The resulting 200-nm-thick polymer layer can be seen in Fig. 2(a) and 2(b), although its uniformity along the length of the channel was difficult to ascertain by SEM.

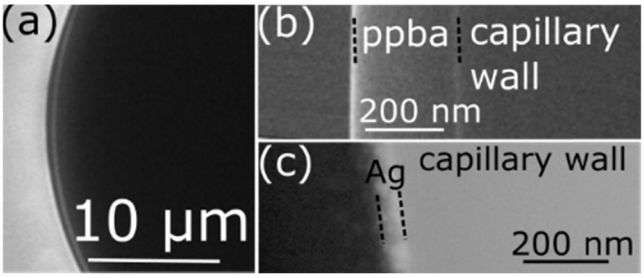

Fig. 2. (a) Low-magnification SEM image showing the polymer-coated capillary channel. (b) A zoom-in of the interface showing the ~230-nm-thick ppba high-index coating. (c) Same as in (b) except with the Ag mirrors. The Ag coating appears bright against the capillary wall and is ~30 nm thick. These images were taken by cleaving the capillary and imaging it using a Zeiss Sigma 300 VP-FESEM operated at 25 keV in either backscatter or secondary electron mode.

An electroless plating method was used to deposit a silver film inside the capillary channel via the precipitation of metallic silver from ammoniacal silver nitrate solution in the presence of a reducing agent (*i.e.* Tollens' reaction). First, tin(II) chloride (0.1 M of $SnCl_2$ in 0.1 M of HCl) solution was flowed into the capillary to promote film adhesion onto the fused silica capillary walls [32] using a syringe pump at a constant flow rate of 50 μL/min for 5 min. The preparation of Tollens' reagent started with the oxidation of an aqueous silver nitrate solution (0.24 M) into silver oxide using potassium hydroxide (0.25 M), resulting in the formation of a brown precipitate. Ammonia (3 M) was then added dropwise to the solution to dissolve the silver oxide and produce a transparent silver ammonia complex.

Once the silver ammonia complex became colorless, the reducing agent (1:2 mixture of methanol and 1.9 M glucose) was added to Tollens' reagent to cause the reduction of the silver ammonia complex. This solution was then pumped through the capillary for 4 minutes in order to achieve a silver channel coating a few tens of nm thick. Tollens' reaction also successfully produced a capillary channel coating, with the Ag about 30 nm thick, as seen in Fig. 3(c), and fairly rough, consistent with previous results on cover slips and optical fibers [33].

The capillaries were then attached to polytetrafluoroethylene tubing and mounted over an objective lens. Light from a tungsten lamp was focused onto one side of the capillary, transmitted through the structure, and the spectrum was projected onto a miniature spectrometer [Fig. 1] with a pitch of 0.077 nm/pixel on the CCD. The capillary was precisely aligned parallel to the spectrometer entrance slit, which was centered along the capillary axis. A gas tubing interface was used to force gases through the capillary at controllable pressures while the optical transmission spectra were being collected. Liquid experiments used a syringe pump to inject sucrose-water mixtures into the capillary at a flow rate of 5 μL/min.

Finite-difference time domain (FDTD) simulations using the commercial OmniSim package were performed to validate the experimental data. The domain size was 50 nm, with

Optics EXPRESS

perfectly matched layers at the boundaries of the simulation domain. The emitter produces a simulated sinusoidal plane wave (in order to match the experiment reasonably well) with a pulse length of 5 fs in order to give a wide spectral range. The simulated time was at least 200 ps, by which time the electric field amplitude in the device had decreased to negligible values. For full devices, a single simulation run took ~4 hours on a 2.4 GHz PC using 15 cores.

4. Experimental results

4.1 Polymer-coated channels

The transmission spectrum for a capillary with a polymer channel coating (with air both in the channel and outside the capillary) showed a complex set of overlapping cavity resonances [Fig. 3], as expected for the four dielectric interfaces. The Fourier spectrum contained at least four high-power regions whose mean free spectral range (FSR) can be determined according to $\Delta\lambda_{spec}/K$, where $\Delta\lambda_{spec}$ is the spectral width in Fig. 3 and K is the peak Fourier component number. Accordingly, one can extract four main periodicities having mean FSRs of 3.6, 0.92, 0.72, and 0.40 nm. The FSRs calculated according to $\Delta f = c/(2n_{eff}L)$ for cavities 2-3, 1-2, 1-3, and 1-4 can be estimated using the mean refractive index (*i.e.,* spatially averaged along the path length) for n_{eff}. This gives FSRs of 3.6, 0.91, 0.73, and 0.41 nm, respectively, in reasonably good agreement with observation. The resonances have a somewhat broad Fourier power spectrum because the mode spacing is not perfectly uniform in wavelength units.

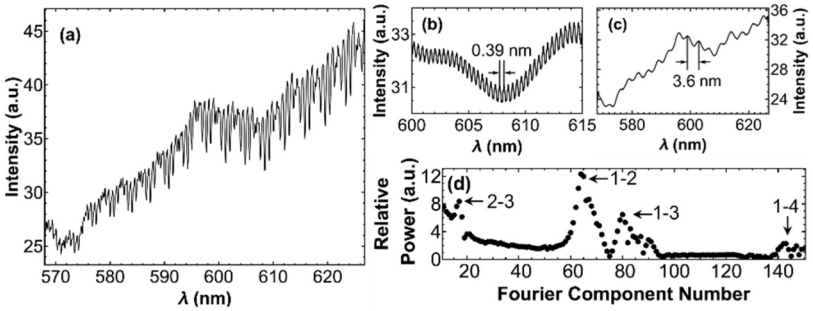

Fig. 3. (a) Raw transmitted light spectrum showing several overlapping oscillations. (b) Transmission spectrum taken with mineral oil in the channel. Only the high-frequency oscillations corresponding to the cavity defined by interfaces (1-4) are visible. (c) The mode spectrum for the same capillary (with air in the channel) immersed in mineral oil in order to remove interfaces 1 and 4. The low-frequency oscillations with a spacing of 3.6 nm correspond to interfaces (2-3). (d) A Fourier power series for the raw transmitted light spectrum. The arrowed peaks correspond to the cavity defined by the associated interfaces.

To confirm these mode identifications, mineral oil (n = 1.45, Sigma) was used as an index matching fluid. When the mineral oil was pumped into the channel (with air on the outside), the only observable modes had a periodicity of 0.39 nm, consistent with a cavity formed by the outer interfaces (1-4) only [Fig. 3(b)]. The observed Q-factor for these modes ($Q = \lambda_0/\Delta\lambda_{FWHM}$ = ~3000) appears higher than the theoretical value calculated as described above $Q = (2\pi L/(-\lambda \cdot Ln[R]))$ = 1400, but due to extensive mode overlap the measurement clearly underestimates the measured peak width ($\Delta\lambda_{FWHM}$). To further support the mode identifications, the capillary was next immersed in mineral oil, thus effectively removing interfaces 1 and 4, while the channel contained air. Two holes were drilled into opposite faces of a cuvette. The capillary was inserted through these holes, which were then sealed with adhesive, so that a section of the capillary was inside the cuvette. The cuvette was then filled with mineral oil and capped. In this case, the only observable modes had a periodicity of 3.6 nm [Fig. 3(c)], confirming that they are indeed the channel modes. The observed Q-factor was 225, which is similar to the predicted value of 200 for the polymer-coated channel.

Optics EXPRESS

The channel modes are especially applicable for refractometric sensing applications. To demonstrate this, Ar and N_2 gas (99.998% purity) were flowed sequentially through the capillary channel at a pressure of 170 kPa. A channel mode spectrum was collected every 23-46 seconds and the resonance shifts associated with the channel modes were measured using the Fourier shift technique [34] [Fig. 4], taking the main Fourier component only to avoid possible overlaps with other modes.

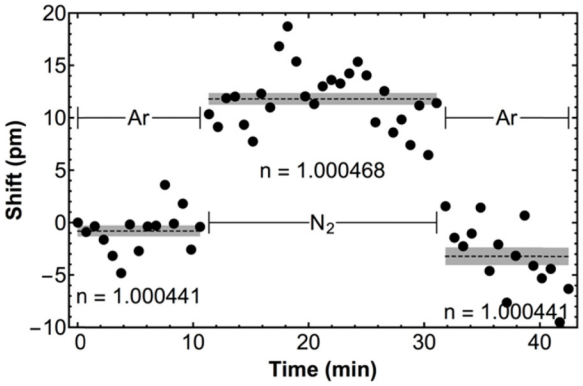

Fig. 4. Refractometric sensorgram on transitioning from Ar to N_2 and back to Ar. Only the main Fourier component for interface 2-3 was used to calculate the spectral shifts. The grey boundaries are centered on the mean and their thickness represents the standard error of the mean. The refractive indices of Ar and N_2 are also shown, as calculated from the Gladstone-Dale equation. The fact that the final Ar result did not precisely return to the original one within the standard error of the mean is likely due to a systematic (drift) error, possibly caused by mechanical drifts that were difficult to eliminate when changing gases.

The refractive index of Ar at a pressure of 170 kPa (10 psi gauge pressure) can be estimated from the Gladstone-Dale approximation of the Lorentz-Lorenz law given by $n = 1 + \mu(P/T)$ where μ is a gas-dependent constant equal to 762 x 10^{-9} and 808.8 x 10^{-9} K/Pa for Ar and N_2, respectively [35], and P and T are the pressure and temperature. Accordingly, the refractive index increases by ~2.7 x 10^{-5} RIU on transitioning from Ar to N_2 at this pressure. This transition was readily detectable in the sensorgram [Fig. 4], which demonstrated a mode shift of 12.6 ± 0.3 pm on going from Ar to N_2. The uncertainties were obtained from the standard error of the mean for each step, with uncertainties for each step added in quadrature. This yields a refractometric sensitivity, S, of (4.7 ± 0.3) x 10^2 nm/RIU at a wavelength near 600 nm. The relatively large error in the sensitivity is due to the data scatter in Fig. 4.

The LoD is typically estimated with 99.7% certainty according to $3\sigma/S$, where σ represents the standard deviation of the wavelength shifts under constant conditions. From Fig. 4, the LoD is therefore (1.3 ± 0.1) x 10^{-5} RIU. This experimentally-detected change compares favorably with the calculated LoD for recently-developed square capillary devices [36]. However, in typical runs in which it was not necessary to switch gases (and thereby induce pressure fluctuations and mechanical motion), a better 3σ shift resolution was obtained, down to 3.5 pm (an example is shown in Fig. 5); accordingly under conditions like those in Fig. 5 the device has an LoD of ~(7.6 ± 0.5) x 10^{-6} RIU at a wavelength of ~600 nm. Despite its simplicity, the optimum detection limit is comparable to those of the best microscale refractometric devices such as whispering gallery mode [16,34] and surface plasmon sensors [37].

Finally, a polymer-coated capillary can also serve as a sensitive gas pressure sensor. To demonstrate this, a capillary was filled with Ar at a pressure of 301 kPa and the resonance wavelengths were monitored as the pressure was increased to 401 and then 501 kPa [Fig. 5]. The modes redshifted by ~140 pm owing to the pressure dependence of the refractive index of argon as articulated by the Gladstone-Dale equation given above. The results yielded a shift

Optics EXPRESS

of 4.88 ± 0.01 pm/psi = 0.709 ± 0.002 pm/kPa at a wavelength of ~600 nm, which is close to an order of magnitude better than currently-reported state-of-the-art FP-type gas pressure sensors [38] and is similar to the exceptional response of a just-published fiber sensor [39] that lacks the simple flow capacity shown here. The latter studies used air, which displays similar pressure-related behavior to both Ar and N_2, validating these comparisons. From the mode shift deviations under constant conditions, we find a pressure-related LoD of 4.96 ± 0.01 kPa.

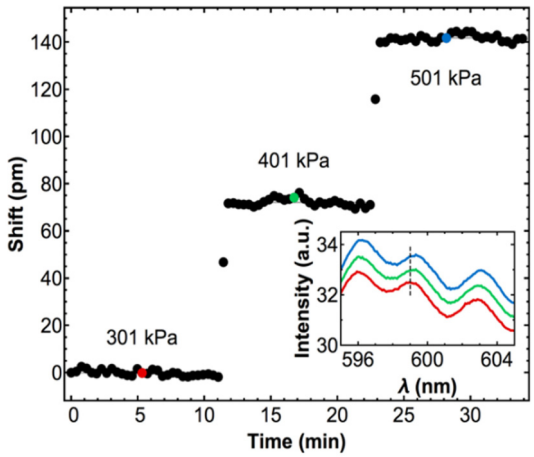

Fig. 5. Pressure sensorgram showing the mode shifts as the pressure was changed twice and then held for ~11 min. Only the main Fourier component ((2-3) in Fig. 3) was used to calculate the spectral shifts. The inset shows a portion of each transmission spectrum on increasing pressure from bottom (red) to top (blue). The colors refer to the specific spectrum indicated by the colored points on the main panel. The standard error of the mean is < 2pm and is smaller than the data points. The refractive indices estimated from the Gladstone-Dale approximation are 1.00077, 1.00103, and 1.00128 for the three increasing pressures shown.

Liquid sensing is also particularly interesting for a large range of applications. However, the mode visibility of the polymer coated capillary dropped significantly once filled with liquid, to the point where clear sensorgrams couldn't be obtained. The poor mode visibility was attributed to the relatively low refractive index contrast between the polymer coating and water in the capillary channel. It is negligibly influenced by the capillary wall thickness, as one effectively satisfies the "thick substrate" criterion for capillaries of these dimensions.

4.2 Silver-mirrored channels

The channel mode visibility with air in the channel was much higher for the silver mirrors [Fig. 6] than for the polymer coating, due to the higher reflectivity. The FSR was close to 3.6 nm near λ = 600 nm, again consistent with the 2-3 resonances. Transfer matrix calculations showed that the reflectivity of a flat, 30-nm-thick silver mirror is 87.6% and 84.8% in air and water, respectively, yielding calculated Q factors on the order of 4000. Experimentally, the Q factors were ~413; these significantly lower values are probably due to scattering induced by the high surface roughness of the deposited silver coating as shown previously [33].

In order to test the response of the Ag-mirrored capillaries, a new pressure sensorgram was taken using Ar in the channel [Fig. 7(a)]. Here the pressure was varied from 301 to 501 kPa in 40 kPa steps. The silver-mirrored capillary tracked these pressure changes well; by using the Gladstone-Dale approximation described above we obtain a pressure sensitivity of 1.08 ± 0.04 pm/kPa corresponding to an RI sensitivity of (4.2 ± 0.2) x 10^2 nm/RIU. The uncertainty comes from the linear fit to the data in the inset to Fig. 7(a), where we ignore the error in the pressure measurements as probably smaller than the relative error in $\Delta\lambda$. The LoD

Optics EXPRESS

calculated from the measured sensitivity and the optimum system resolution (most stable run, where 3σ = 3.5 pm as described above), was 3.3 ± 0.1 kPa.

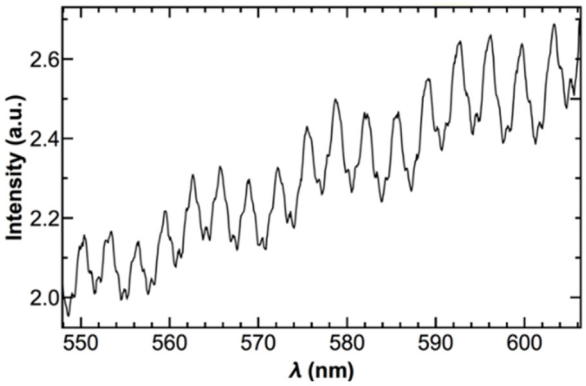

Fig. 6. Transmission spectrum through the center of a silver-mirrored microcapillary, with Ar in the channel. The spectrum is dominated by a set of modes with an FSR of ~3.6 nm.

Unlike the polymer-coated capillary, the silver-mirrored one can also readily function as a liquid sensor [Fig. 7(b)]. Whereas for the polymer coating the 2-3 mode visibility became too small, the Ag mirrors retained a high reflectivity and therefore good mode visibility for liquid channel media also. Here, the refractometric sensitivity was found to be 354.2 ± 0.6 nm/RIU for sucrose-water solutions, yielding a best-case 3σ detection limit of (1.000 ± 0.002) x 10^{-5} RIU.

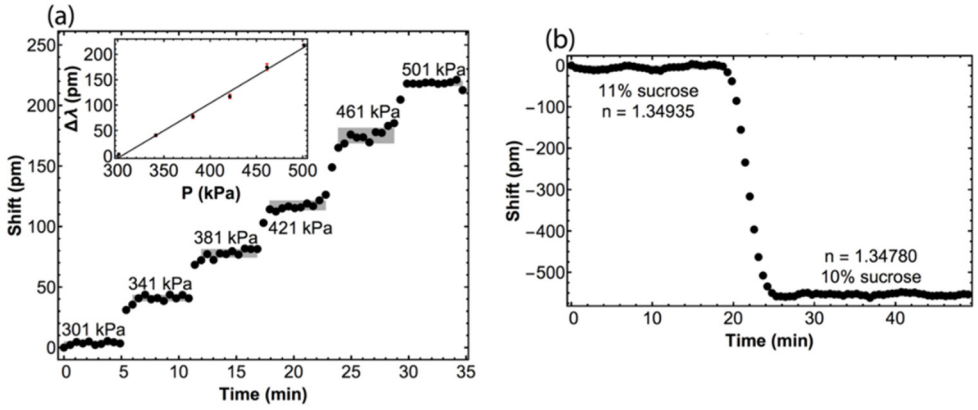

Fig. 7. (a) Pressure sensorgram for Ar gas in a silver-mirrored capillary. The inset shows a linear fit to the mean resonance shifts, yielding a pressure sensitivity of 1.07 ± 0.02 nm/RIU. (b) Sensorgram as two concentrations of sucrose (11% w/w and 10% w/w) solution are pumped through the capillary

5. Comments and discussion

The resonance wavelength of an FP cavity is given by $\lambda_0 = 4\pi nL\cos\theta/(2\pi m + \phi_1 + \phi_2)$, where L is the cavity length, θ is the incidence angle, m is the order, and ϕ_1 and ϕ_2 are the phase shifts on reflection at the two interfaces. Accordingly, the refractometric sensitivity of an ideal capillary FP cavity with m>>1 is given by $S = dn/d\lambda \approx 4R/m$, where R is the capillary radius as before. There is no dependence on the reflectivity of the mirrors or the quality factor of the cavity. Mirror roughness (see Fig. 2) also doesn't matter insofar as the sensitivity is concerned, although it can decrease the visibility and thereby degrade the mode shift resolution and the LoD. Thus, the deciding factor controlling the refractometric sensitivity for

Optics EXPRESS

these capillary sensors is the measurement wavelength, because it determines *m* independently of the radius (in other words, for a fixed resonant wavelength, there are many possible combinations of *L* and *m* but they all have the same refractometric sensitivity).

Using $S = 4R/m$, one predicts a refractometric sensitivity of 599 nm/RIU for both the polymer- and silver-mirrored channel near λ = 600 nm and n = 1.002 (Table 1). We observed $(4.7 \pm 0.3) \times 10^2$ and $(5.6 \pm 0.2) \times 10^2$ nm/RIU for the polymer and silver-mirrored capillaries, respectively. The experimental sensitivities tended to be somewhat lower than the theoretical values. One possible reason is that the Gladstone-Dale approximation used to calculate the RIs may overestimate the RI difference between Ar and N_2 at the measurement pressure.

A few other comments can also be made at this point. First, we see that the refractometric sensitivity is lower with liquid in the channel as compared to gas. At a fixed wavelength, increasing the RI of the channel medium increases the mode order correspondingly, thus lowering the sensitivity (opposite to the case of a WGM resonator, in which the sensitivity decreases for *lower* analyte index). These observations are also in agreement with the general trends predicted by the analysis above.

However, some discrepancies also exist. For example, the liquid sensitivity for Ag-mirrored channels (Table 1) is about 63% of the gas one, but the theory implies that it should be 75% of it (according to the ratio of channel refractive indices 1.00:1.33). Also, the lower "pressure LoD" for the Ag mirrored devices as compared to the polymer ones is unexpected; from the above discussion one would expect them to be the same. We can't unambiguously explain this discrepancy, but we note that the Fourier spectra (from which the wavelength shifts are calculated) were much weaker in the polymer case than they were in the Ag one, due to the much lower visibility of the 2-3 resonances and the maximum-power component was not nearly as well defined. These differences affect the accuracy of the Fourier shift method [34] and could potentially be responsible for the different observed pressure LoDs (3.3 vs. 5.0 kPa for Ag and ppba mirrors, respectively).

Table 1. Summary of the experimental, simulated, and calculated sensitivities of polymer-coated and silver-mirrored capillaries in nm/RIU. Listed values are for wavelengths of 600 nm and 1550 nm, and near RIs of 1.002 (air) or 1.33 (water). Units are nm/RIU.

			Experiment	FDTD	Theory
600 nm	Poly	Air	468	530	599
		Water	–	420	452
	Ag	Air	565	516	599
		Water	354	412	452
1550 nm	Poly	Air	–	1574	1547
		Water	–	1128[a]	1165
	Ag	Air	–	1513	1547
		Water	–	1222	1165

[a]The FDTD result for water in the polymer-coated channel yielded low-visibility, low–Q modes that were difficult to analyze by Fourier methods, so the peak shift was estimated manually by choosing the highest point.

A brief discussion of the error analysis appears necessary. The device sensitivities were calculated from the experimental wavelength shifts, which were obtained as the difference in the mean values of $\Delta\lambda$. The reported uncertainties come from quadrature addition of the standard error of the means ($SE = \sigma/n^{0.5}$), where σ is the sample standard deviation and n is the number of measurements for each shift value. The fact that the uncertainties are far smaller than the nominal "resolution" of the spectrometer isn't inconsistent because they simply come from the noise in the mode peak positions under constant conditions. For several of the runs, these values were very small, with a standard deviation of less than 1.5 pm. This error analysis does, however, ignore systematic errors which we do believe are significant but are difficult to quantify.

Since most of the Fabry-Pérot fiber sensors cited in the literature were tested at a wavelength near 1550 nm, the sensitivity in the infrared would present a more consistent

Optics EXPRESS

comparison with previous work. For Fabry-Pérot-type cavities, the wavelength shift under a fixed index change is directly proportional to the central wavelength. Thus, at 1550 nm the sensitivity of the capillary device would be close to 1540 nm/RIU for air in the channel. This estimate is in reasonable agreement with FDTD simulations which gave a sensitivity of 1574 nm/RIU.

The best detection limit we could achieve was (6.3 ± 0.2) x 10^{-6} RIU, taking the most stable experimental run to calculate the 3σ variation in the mode peak positions. The detection limit varies inversely with wavelength, due to the greater sensitivity of the proportionally smaller mode orders. Thus, at 1550 nm (as compared to 600 nm for the current measurements) the detection limit is predicted to be 2.3 x 10^{-6} RIU, which is also in excellent agreement with FDTD simulations.

Temperature cross-sensitivity is an issue for many sensors [40,41]. The response to temperature fluctuations is due to thermal expansion which for silica is 5.5 x 10^{-7} K^{-1} [42], giving a relative change of a few parts in 10^5 for a temperature change of 100 °C, corresponding to a few pm of spectral drift. Since this is quite close to the shift resolution, one can conclude good thermal stability over a range of ~100 °C, but for larger temperature drifts the thermal expansion would have to be compensated. Of course, in an open system the thermo-optic coefficient of the gas would cause a change in the RI which may not be distinguishable from a change in pressure; whereas in a closed system both P and T would change concurrently and the effects would cancel insofar as one has an ideal gas.

There are several additional features of this device. No splicing, melting, femtosecond laser ablation [10,39], or nanolithography is required as is usually the case for other sensors. Since the mode propagates mainly in the channel, the elasto-optic effect, which can be a problem for fiber sensors, is not important here. The compressibility of silica near atmospheric pressure is 9.8 x 10^{-12} Pa^{-1} [43], which would cause a redshift of a fraction of a picometer due to elastic expansion in this pressure range. The compressibility of ppba is unknown but the values for related polymers such as PMMA are on the order of 1.5 x 10^{-10} Pa^{-1} [44], and for silver it is ~1 x 10^{-11} Pa^{-1} [45]. These values are about an order of magnitude larger than that of silica but would still cause negligibly small mode shifts as compared to the wavelength shift resolution (*i.e.*, the polymer film thickness would change by a few parts in 10^5 over 200 kPa leading to a few pm of spectral drift, around 1% of the typical changes observed).

However, similar to other FP gas sensors, gas specificity is currently lacking. One can envision ways to overcome this problem in the future, such as, for example, by filling a capillary with a porous absorber. Indeed, this concept has recently been demonstrated for fluid biosensors [46]. Secondly, a small amount of heating is likely to occur in the sample. We did not make any temperature-stabilizing efforts here; but since the device only uses a comparatively weak white light source, thermal drifts should be minimal. Indeed, after the sample was allowed to stabilize for a few minutes we found no observable thermal drift in the reported sensorgrams after starting an experiment.

A final question concerns the value of a capillary-type FP sensor as compared to the fiber-optic sensors investigated previously. First, despite its simplicity a mirrored-capillary gas, liquid, and pressure sensor hasn't been shown before. In fact, the simplicity of the device is an attractive aspect since only a very straightforward fabrication is required and it could easily be parallelized to produce multiple devices. Secondly, sensitivity in the visible spectrum is as good as or better than in previously demonstrated FP devices, with predicted detection limits in the low 10^{-6} RIU range at a wavelength of 1.55 μm. Third, the light source is nothing more than a simple incandescent bulb. Finally, better mechanical stabilization (*e.g.*, by packaging the capillary and light source) would likely lead to a smaller shift resolution and even better detection limits.

Optics EXPRESS

6. Conclusions

To conclude, we show a simple, robust refractometric gas sensor based on a capillary coated with a high-index polymer or metallic silver. The response is comparable to or better than many other optical gas sensors. A refractometric shift of 2.7 x 10^{-5} RIU was tested and an optimum detection limit of (6.3 ± 1.1) x 10^{-6} RIU was found at a wavelength of ~600 nm. These values would further improve by a factor of ~2.6 at the infrared wavelengths used by other detection systems. The device can also function as a gas pressure sensor with a detection limit as low as 3.3 ± 0.1 kPa at λ = 600 nm, which is comparable to the best optical pressure sensors reported to date. The concept doesn't require any complicated equipment or preparation. The same concept was demonstrated for fluid sensing in the channel as well, again with competitive sensitivities and LoDs. The results were finally discussed in terms of the simple theory governing the sensitivity of FP-type refractometric sensors.

Funding

Natural Science and Engineering Research Council of Canada (NSERC) CREATE Program (grant 463990-2015); Australian Research Council (ARC) Georgina Sweet Laureate Fellowship.

Acknowledgments

We thank Sergei Vagin (Technische Universität München) for discussions on high-index polymers.